Correlation and localization properties of topological charge density and the pseudoscalar glueball mass in SU(3) lattice Yang-Mills theory

Abhishek Chowdhury,[1,*] A. Harindranath,[1,†] and Jyotirmoy Maiti[2,‡]

[1]*Theory Division, Saha Institute of Nuclear Physics, 1/AF Bidhan Nagar, Kolkata 700064, India*
[2]*Department of Physics, Barasat Government College, 10 KNC Road, Barasat, Kolkata 700124, India*

(Received 9 January 2015; revised manuscript received 11 March 2015; published 8 April 2015)

In order to extract continuum properties, we study the topological charge density correlator (TCDC) and the inverse participation ratio (IPR) for the topological charge density $q(x)$ in SU(3) lattice Yang-Mills theory for relatively small lattice spacings, including some smaller than those explored before. With the help of a recently proposed open boundary condition, it is possible to compute observables at a smaller lattice spacing since the *trapping problem* is absent. On the other hand, the reference energy scale provided by the Wilson flow allows us to study their scaling behavior, in contrast to previously proposed smearing techniques. The behavior of the TCDC for different lattice spacings at a fixed hypercubic smearing level shows apparent scaling violations. In contrast, at a particular Wilson flow time t for all of the lattice spacings investigated (except the largest one), the TCDC data show universal behavior within our statistical uncertainties. The continuum properties of the TCDC are studied by investigating the small-flow-time behavior. We also extract the pseudoscalar glueball mass from the TCDC, which appears to be insensitive to the lattice spacings ($0.0345\ \text{fm} \leq a \leq 0.0667\ \text{fm}$) and agrees with the value extracted using anisotropic lattices, within statistical errors. Further, we study the localization property of $q(x)$ using the IPR (whose continuum behavior can be probed using small values of the Wilson flow time) and observe a decrease of the IPR with decreasing Wilson flow time. A detailed study of $q(x)$ under the Wilson flow time reveals that as the Wilson flow time decreases, the proximity of the regions of positive and negative charge densities of large magnitude increases, and the charge density appears to be more delocalized, resulting in the observed behavior of the IPR.

DOI: 10.1103/PhysRevD.91.074507 PACS numbers: 11.15.Ha, 11.15.-q, 12.38.-t, 12.38.Gc

I. INTRODUCTION AND MOTIVATION

The negativity of the topological charge density correlator (TCDC) for nonzero distances—which is a consequence of the reflection positivity and the pseudoscalar nature of the relevant local operator in Euclidean field theory—is well known [1,2]. The nontrivial implication of the negativity of the TCDC for the structure of the topological charge density in the QCD vacuum has been investigated in detail [3]. Various aspects of the TCDC in quenched and full QCD were carried out in Refs. [4–13]. The four-volume integral of the TCDC gives the topological susceptibility χ. A thorough investigation of the mechanisms leading to the suppression of the topological susceptibility with decreasing quark mass based on the properties of the TCDC was carried out [11] in two-flavor QCD. The famous Witten-Veneziano formula [14,15] relates the mass of η' to the topological susceptibility in pure Yang-Mills theory.

Various definitions for the calculation of the topological charge density $q(x)$ have been used in the literature. Reference [16] used the algebraic definition of the field-strength tensor. To overcome the potential lattice artifacts associated with the algebraic definition of the topological charge density $q(x)$ on the lattice and severe singularities present in the TCDC in the continuum theory, various proposals have been studied in the literature. In Ref. [17], $q(x)$ based on Ginsparg-Wilson fermion was employed, whereas Refs. [18,19] utilized a proposal designed to overcome short-distance singularities. A spectral projection formula designed to be free of singularities was employed in Ref. [20], which compared the result for the topological susceptibility χ using the algebraic definition. Since Ref. [20] has established that the results for χ using various approaches are in agreement with one another within statistical uncertainties, in this work we employ the algebraic (clover) definition for $q(x)$ unless otherwise stated.

There remain several open issues related to the topological charge density $q(x)$ and the TCDC in non-Abelian gauge theories. An important issue is the scaling of the TCDC as one approaches the continuum limit. However, it is well known that current lattice gauge theory simulations that employ periodic boundary condition in the temporal direction are handicapped by the trapping of topological charge in a particular sector, as the lattice spacing is reduced so as to reach the continuum limit. An open boundary condition in the temporal direction has been

*abhishek.chowdhury@saha.ac.in
†a.harindranath@saha.ac.in
‡jyotirmoy.maiti@gmail.com

proposed and investigated [21–23] as a (partial) cure to this problem. An open boundary condition has also been used advantageously in the investigation of SU(2) lattice gauge theory at weak coupling in Ref. [24]. With the open boundary condition, one can probe the TCDC for even smaller lattice spacings and address questions related to the scaling, etc.

With the adoption of the algebraic definition of $q(x)$, to suppress unwanted lattice artifacts a smearing of the gauge fields is necessary. In our previous study of the TCDC [11], we employed hypercubic (HYP) smearing [25]. However, recently proposed Wilson flow [26–28] makes smearing a well-defined mathematical procedure, and also provides a common reference scale to extract physical quantities from lattice calculations employing different lattice spacings. The continuum properties of observables such as the TCDC can be studied by investigating the small-flow-time behavior. The scale provided by the Wilson flow has been used in pure Yang-Mills theory to compare topological susceptibilities calculated at different lattice spacings [29]. A similar scaling study for topological susceptibility was recently performed for dynamical fermions [12].

With the help of the open boundary condition, we have been able to extract [30] the scalar glueball mass down to a lattice spacing of 0.0345 fm, which was not accessible with periodic boundary condition. It will also be very interesting to extract the pseudoscalar glueball mass with the same ensembles of configurations from the tail region of the TCDC.

In addition to the properties of the correlator of the topological charge density, the localization property itself is also of interest. There exists a body of literature on the localization properties of the low-lying Dirac eigenmodes [31], due to their connection with the topological properties of the QCD vacuum. However, the localization properties of the topological charge density based on the algebraic definition involving the field strength $F_{\mu\nu}$ seems to have attracted little attention, except for a preliminary study by the MILC Collaboration [32]. It is interesting to study the inverse participation ratio (IPR) associated with the topological charge density distribution and analyse its behavior under the Wilson flow and HYP smearing. A direct visualization of the effect of the Wilson flow on the topological charge density distribution of typical gauge configurations will also shed light on their localization properties.

II. SIMULATION PARAMETERS

In Table I we present simulation parameters for the hybrid Monte Carlo (HMC) algorithm used to generate configurations with open and periodic boundary conditions in the temporal direction with the unimproved SU(3) Wilson gauge action. We also give the number of configurations used for measurements of the TCDC and IPR. The "Gap" multiplied by τ denotes the trajectory interval between two successive measurements. We have chosen the gaps from our studies of the autocorrelation for the TCDC at a fixed value of r (in units of fm), such that the measurements are statistically independent of one another. The ensemble P_3 is an exception because—due to the significantly smaller ensemble size in this case (which is due to the larger value of β and the periodic boundary)—it was not possible to maintain large enough gaps between successive measurements. Hence, in this case errors are somewhat underestimated. Lattice spacings for different ensembles are determined using the results from Refs. [33,34].

With the periodic boundary condition, source averaging is usually performed for the measurement of the TCDC in order to increase statistics. However, with the open boundary condition this cannot be done, as translational invariance is lost in the temporal direction. In order to avoid boundary effects in this case, the source is kept at the midpoint of the temporal extent while calculating the TCDC, and an averaging over the spatial volume is performed. For a meaningful comparison between the results for open and periodic lattices, we adopt the same source averaging procedure for the latter case as well.

III. NUMERICAL RESULTS

A. Topological charge density correlator

The TCDC is given by

$$C(r) = \langle q(x)q(y)\rangle, \qquad r = |x-y|, \tag{1}$$

TABLE I. Simulation parameters for the HMC algorithm. O and P refer to ensembles with open and periodic boundary conditions in the temporal direction, respectively. N_{cnfg} is the total number of measurements, "Gap" denotes the interval between two successive measurements in units of τ (the molecular dynamics trajectory length), and t_0/a^2 is the dimensionless reference Wilson flow time.

Lattice	Volume	β	N_{cnfg}	Gap	τ	a [fm]	t_0/a^2
O_1	$24^3 \times 48$	6.21	401	392	3	0.0667(5)	6.207(15)
O_2	$32^3 \times 64$	6.42	405	240	4	0.0500(4)	11.228(31)
O_3	$48^3 \times 96$	6.59	458	160	5	0.0402(3)	17.630(53)
O_4	$64^3 \times 128$	6.71	74	160	10	0.0345(4)	24.279(227)
P_1	$24^3 \times 48$	6.21	401	280	3	0.0667(5)	6.197(15)
P_2	$32^3 \times 64$	6.42	401	176	4	0.0500(4)	11.270(38)
P_3	$48^3 \times 96$	6.59	191	64	5	0.0402(3)	18.048(152)

where $q(x)$ is the topological charge density. In order to extract the continuum properties of the TCDC from lattice simulations, a smoothing of the gauge fields is necessary if one uses the field-theoretic definition of the topological charge density. Unlike observables (such as hadron masses and topological susceptibilites), the properties of the TCDC depend on the energy scale at which one is probing the system. Thus when we compare the TCDC at different lattice spacings using smeared gauge configurations, we have to ensure that the smearing is performed at a given energy scale.

In conventional smearing techniques like HYP smearing, a fixed smearing level does not correspond to a common energy scale, which could be used to compare data generated at different lattice spacings. In Fig. 1, the TCDCs at various lattice scales are compared at the same HYP smearing level (i.e., level 3). From the exhibited behavior one may infer large scaling violations, but one should keep in mind that a fixed HYP smearing level at different lattice spacings does not correspond to a common energy scale. This is to be contrasted with the Wilson flow case, which facilitates the use of a common energy scale, as shown in Fig. 2.

Unlike conventional smearing techniques, the Wilson flow provides an energy scale ($\frac{1}{\sqrt{8t}}$) at which observables can be probed. In order to check possible scaling violations in the TCDC, one has to choose a particular Wilson flow time for all the lattice spacings investigated. In Fig. 2, we plot the TCDC for ensembles O_1, O_2, O_3, and O_4 at Wilson flow time $\sqrt{8t} = 0.14$ fm (the rationale for choosing the scale 0.14 fm will be explained later). Except for the data corresponding to the largest lattice spacing, the data show universal behavior within our statistical uncertainties.

Recently, a comparison of the Wilson flow with cooling was performed [35] where a relation between the Wilson flow time and the number of cooling steps was established. We have investigated whether one can phenomenologically establish a relation between the Wilson flow time and the

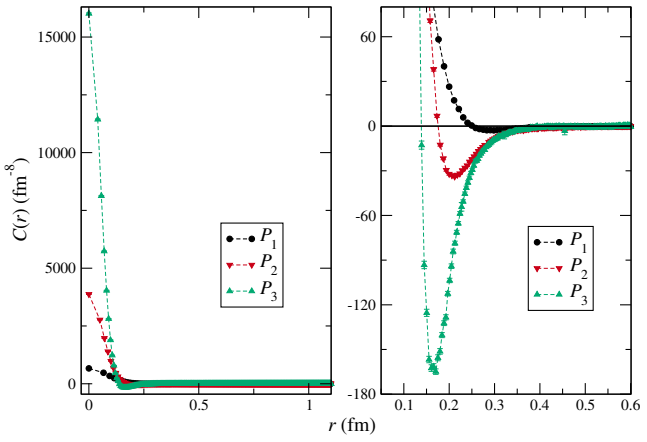

FIG. 1 (color online). $C(r)$ versus r at three HYP smearing steps for ensembles P_1, P_2, and P_3.

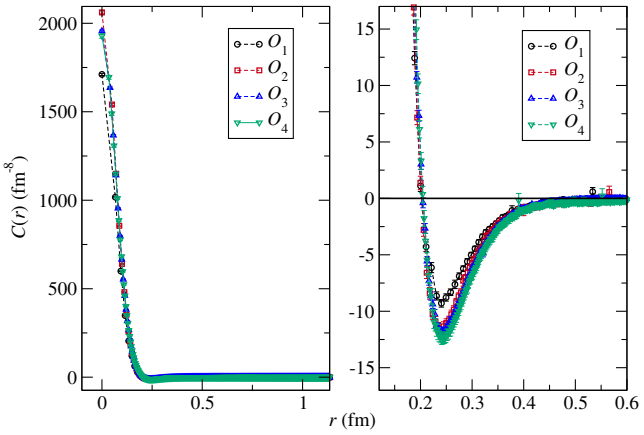

FIG. 2 (color online). $C(r)$ versus r at Wilson flow time $\sqrt{8t} = 0.14$ fm for ensembles O_1, O_2, O_3, and O_4.

HYP smearing level. In the case of the TCDC, we find that it is not possible to establish such a relation even at a fixed lattice spacing, valid for all r. Of course some approximate relation can be found, which, however, will vary with lattice spacing. This issue needs further investigation in the future.

It is expected that the radius of the positive core of $C(r)$ extracted from lattice data shrinks to zero in the continuum limit. In order to investigate this phenomena, we first need to demonstrate the scaling behavior of $C(r)$ extracted at different lattice spacings, and probed at a given Wilson flow time. Then we need to study the behavior of $C(r)$ as the Wilson flow time goes to zero to extract the continuum behavior. In Fig. 3, we plot $C(r)$ versus r at various values of the Wilson flow time $\sqrt{8t}$ at $\beta = 6.42$ and $\beta = 6.59$ for ensembles P_2 (filled triangle) and P_3 (filled square), respectively. At each Wilson flow time, the data corresponding to two different lattice scales give approximately

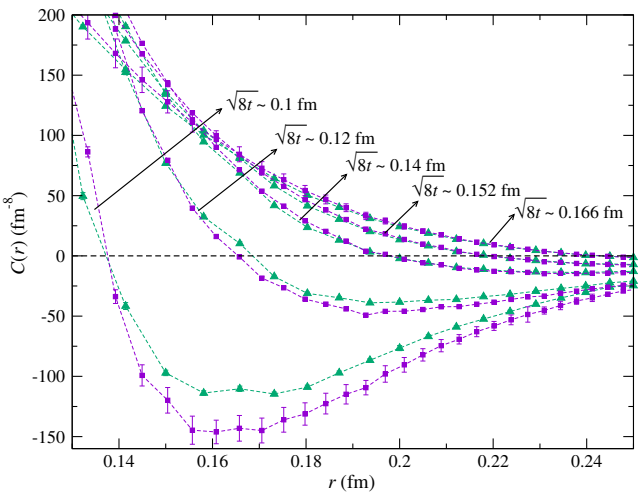

FIG. 3 (color online). Plot of $C(r)$ versus r at various values of the Wilson flow time $\sqrt{8t}$ at $\beta = 6.42$ and $\beta = 6.59$ for ensembles P_2 (filled triangle) and P_3 (filled square), respectively.

the same radius of the positive core of $C(r)$. The agreement is approximate partly because the matching of $\sqrt{8t}$ for two different lattice spacings is approximate. We also observe that the radius of the positive core of $C(r)$ decreases as the Wilson flow time decreases, as expected.

After investigating the scaling behavior, we next explore the properties of $C(r)$ in detail. Without loss of generality, we look at the data at a particular lattice spacing corresponding to $\beta = 6.42$. In Fig. 4, we plot the behavior of $C(r)$ versus r at various Wilson flow times $\sqrt{8t}$ at $\beta = 6.42$ and lattice volume $32^3 \times 64$ for ensemble P_2. The topological charge density (which is constructed from the clover definition of the field-strength tensor) is extended further with the Wilson flow time. As already shown in Fig. 3, the size of the positive core decreases with decreasing Wilson flow time, as presented in Fig. 4. Furthermore, we note that the heights of the positive and negative peaks increase with decreasing flow time. Since the effective size of the charge density increases with increasing flow time, two charge densities eventually overlap, resulting in the complete disappearance of the negative region of $C(r)$.

In Fig. 5, we compare the TCDC for the ensembles P_2 and O_2. We note that there is no noticeable difference between the two TCDCs at a given Wilson flow time. A similar trend has been observed for other lattice spacings as well.

In Fig. 6, we plot the radius of the positive core (r_c) versus Wilson flow time $\sqrt{8t}$ for the ensembles P_2 (filled symbols) and O_2 (open symbols). As noted before, for larger values of the Wilson flow time the TCDC is always positive. As expected, the radius of the positive core r_c diminishes as the Wilson flow time decreases, signaling the behavior expected in the continuum.

In Fig. 7, we plot the unsmeared TCDC for the ensembles O_1, O_2, O_3, and O_4. In this case, the presence of severe lattice artifacts prevents one from extracting any physical observable. For example, one cannot extract the topological susceptibility from such data. Nevertheless, we find that the correlator exhibits negativity, as expected for the correlator of the pseudoscalar operator. Further, we find that the radius of the positive core shrinks with the lattice spacing, as expected.

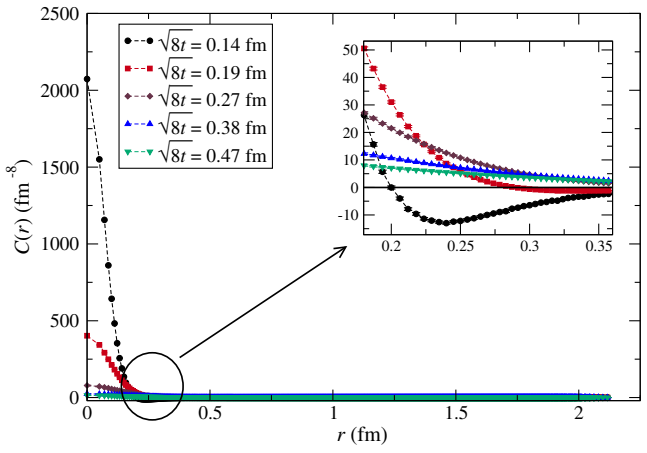

FIG. 4 (color online). Plot of the topological charge density correlator $C(r)$ versus r at various values of the Wilson flow time $\sqrt{8t}$ at $\beta = 6.42$ and lattice volume $32^3 \times 64$ for ensemble P_2.

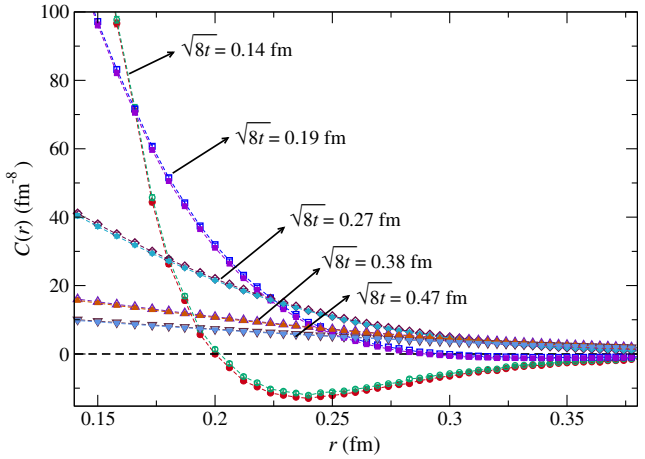

FIG. 5 (color online). Comparison of $C(r)$ versus r at various values of the Wilson flow time $\sqrt{8t}$ at $\beta = 6.42$ and lattice volume $32^3 \times 64$ for ensembles P_2 (filled symbols) and O_2 (open symbols).

B. Extraction of the pseudoscalar glueball mass from the TCDC

Encouraged by the universal behavior exhibited by the TCDC for different lattice spacings at a common Wilson flow time, we proceed to extract the lowest pseudoscalar glueball mass from the tail region of the TCDC. Due to large vacuum fluctuations present in the correlators of gluonic observables, the extraction of glueball masses is much more difficult compared to hadron masses. In QCD,

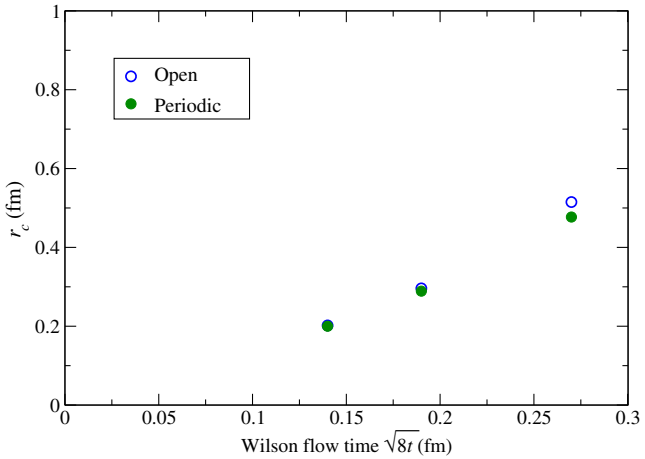

FIG. 6 (color online). Plot of r_c versus Wilson flow time $\sqrt{8t}$ for the ensembles P_2 (filled symbols) and O_2 (open symbols).

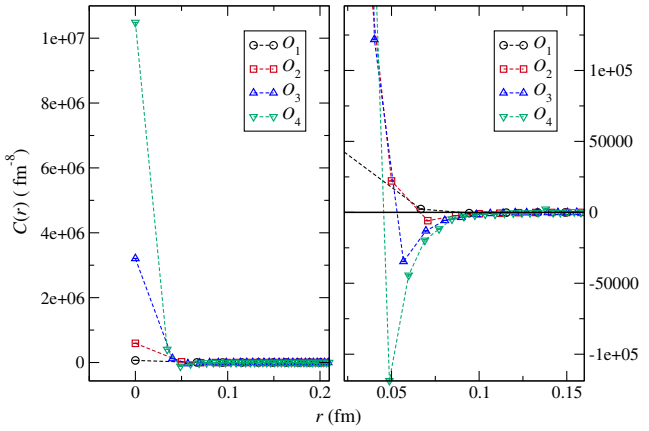

FIG. 7 (color online). Plot of $C(r)$ versus r for ensembles O_1, O_2, O_3, and O_4 without smoothing of the gauge fields.

Ref. [36] proposed the extraction of the pseudoscalar flavor-singlet meson mass from the topological charge density correlator to avoid the complexity of separating connected and disconnected quark diagrams with potentially large statistical fluctuations. In Yang-Mills theory, the extraction of the pseudoscalar glueball mass from the TCDC avoids the same complexity. Since the TCDC has severe singularities and lattice artifacts, a smoothing of the gauge fields is mandatory. Undersmearing of gauge fields leads to persistent lattice artifacts, while oversmearing may wipe out even the negativity character of the correlator. Thus there is an optimal range of smearing for which one can reliably extract useful information from the lattice data. Further, the pseudoscalar glueball mass is expected to be much higher than the scalar glueball mass. Thus one needs larger statistics and lower lattice spacings for the extraction of the pseudoscalar glueball mass. Apart from the cost associated with generating configurations, the cost of measuring the all-to-all radial correlator also increases rapidly as one goes to smaller lattice spacings while keeping the physical volume constant.

In the past, the MILC Collaboration [9] checked the consistency of their quenched correlator data using the pseudoscalar glueball mass extracted in Ref. [37] (which used anisotropic lattices) as an input without actually fitting the data. In this case, a particular level of HYP smearing is used to smooth the gauge configurations at different lattice spacings.

A formula for the TCDC was derived in Appendix B of Ref. [38] for QCD. This is in the context of a leading term in an effective Lagrangian approach originally proposed by Rosenzweig, Schechter, and Trahern [39] and by Di Vecchia and Veneziano [40]. This approach was further developed, being motivated by instanton-inspired considerations. In the analysis of the lattice data, the following functional form [38] of the correlator in the negative region is used to extract the pseudoscalar glueball mass:

$$\langle \phi(x)\phi(y)\rangle = \frac{m}{4\pi^2 r} K_1(mr), \tag{2}$$

where $K_1(z)$ is a modified Bessel function whose asymptotic form is given by

$$K_1(z) \underset{\text{large } z}{\sim} e^{-z}\sqrt{\frac{\pi}{2z}}\left[1+\frac{3}{8z}\right]. \tag{3}$$

In Fig. 8, the TCDC $C(r/a)$ is plotted versus r for the ensemble O_4 at Wilson flow time $\sqrt{8t} = 0.14$ fm. Also shown is the fit in the large-r region with the formula given in Eq. (3) to extract the pseudoscalar glueball mass. In the fitting procedure the amplitude and the mass are treated as free parameters. We studied the stability of the fit results (mass and amplitude) with the fitting range by varying both the initial and final values of r in the tail region of the TCDC.

We have studied the behavior of the extracted pseudoscalar glueball mass under different Wilson flow times. In Fig. 9, we show the sensitivity of the extracted mass to the starting point of the fit range for a chosen end point, for the ensembles P_2 (left) and O_3 (right). The end point is then varied over a very wide range and the stability of the fit for a given starting point is examined. We find that the extracted mass is independent of the end point once the error bar of the tail of the correlator touches the value zero. The extracted mass is apparently stable at and around the scale 0.14 fm, as exhibited in the overlap of the plateau regions of data for three different Wilson flow times. The overlap between the plateau regions is better for the ensemble O_3 compared to the ensemble P_2. This behavior is expected as one approaches the continuum. The extracted mass values for different ensembles are given in Table II. Since the extracted mass is independent of the end point, we do not quote a specific value in the table. As the ensemble sizes for P_3 and O_4 are comparatively small, the

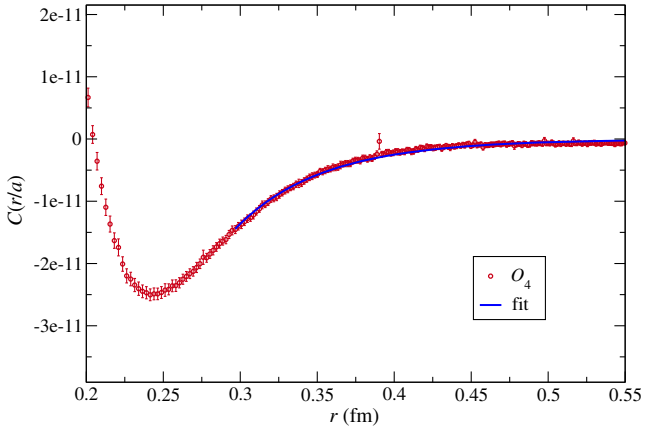

FIG. 8 (color online). $C(r/a)$ versus r for the ensemble O_4 at Wilson flow time $\sqrt{8t} = 0.14$ fm. Also shown is the the fit used to extract the pseudoscalar glueball mass.

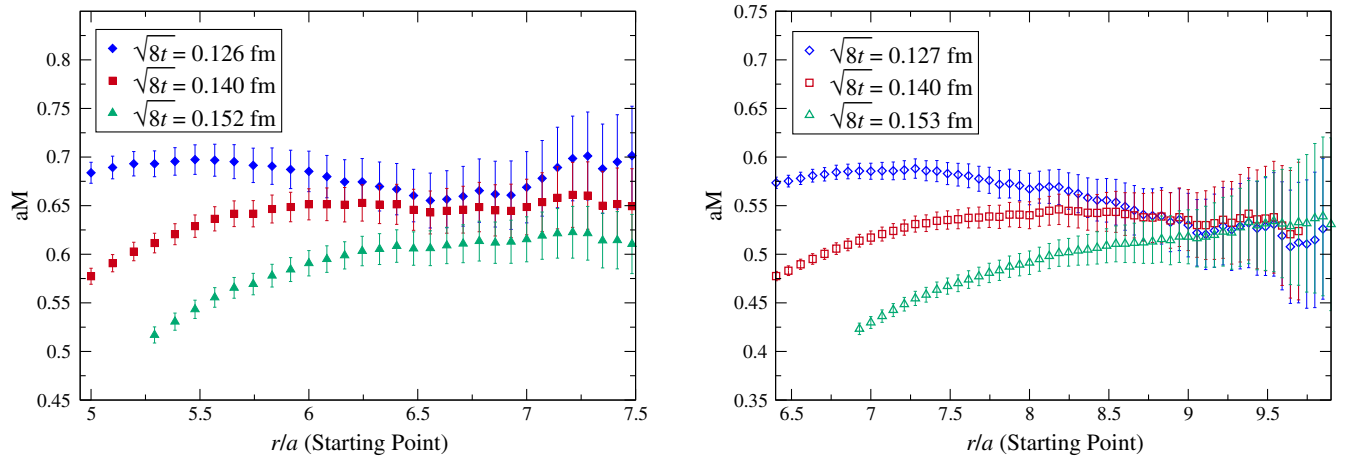

FIG. 9 (color online). Sensitivity to the starting point of the fit range for a fixed end point of the pseudoscalar glueball mass, extracted using the asymptotic formula for ensembles P_2 (left) and O_3 (right).

results for these two ensembles may have some bias, leading to a possible underestimation of errors as well.

In order to extract the pseudoscalar glueball mass in the continuum, in Fig. 10 we plot the mass in MeV versus a^2 in fm^2 for both of the boundary conditions and for all of the lattice spacings explored in this work. As expected from the universal scaling behavior exhibited by $C(r)$ in the asymptotic region (see Fig. 2) within the statistical error, the data for the mass does not show any deviation from scaling. Hence we fit a constant to the data (as shown in the figure) and thus extract the continuum value of the pseudoscalar glueball mass as 2563 (34) MeV. This value compares very well with the value 2560 (35) MeV quoted in Ref. [37], which was extracted from the decay of the temporal pseudoscalar correlator on an anisotropic lattice.

C. Localization properties of the topological charge density

It is interesting to study the localization property of the topological charge density $q(x)$ and its behavior under the Wilson flow. Since the Wilson flow time provides an energy scale to probe the system, it becomes possible to extract the continuum behavior by studying the small Wilson flow time behavior of the observables.

TABLE II. Pseudoscalar glueball mass in lattice and physical units. The starting point of the fit range is denoted by $r_{\rm min}$.

Lattice	$r_{\rm min}$ (fm)	am	m (MeV)
O_1	0.31	0.887(39)	2624(114)
P_1	0.30	0.831(36)	2459(108)
O_2	0.29	0.648(18)	2590(78)
P_2	0.33	0.648(25)	2560(100)
O_3	0.28	0.535(29)	2625(140)
P_3	0.27	0.524(17)	2573(81)
O_4	0.31	0.445(11)	2545(63)

As a measure of the localization property of $q(x)$, one can use the IPR, defined as [31,32]

$$\mathrm{IPR} = V\frac{\sum_x |q(x)|^4}{(\sum_x |q(x)|^2)^2}, \tag{4}$$

where V is the four-dimensional lattice volume. If $q(x)$ is completely local [for example, $q(x) = \delta(x_0)$] IPR $= V$, and if $q(x)$ is completely delocalized [$q(x) = c$, i.e., a constant] then IPR $= 1$. If $q(x)$ is localized on a fraction of sites f then IPR $= \frac{1}{f}$ [32]. Thus the measurement of the IPR provides information about the localization properties of $q(x)$. For an excellent discussion of the IPR [41] (which was originally introduced in the context of condensed matter systems) see Ref. [42].

To investigate the effect of the Wilson flow on the localization property of the topological charge density, we

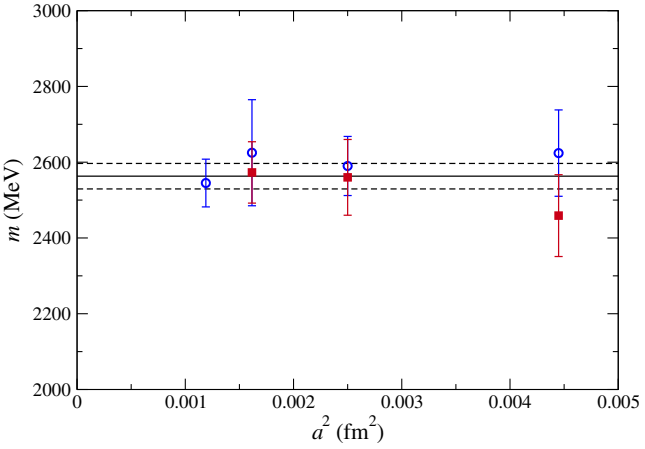

FIG. 10 (color online). Plot of the lowest pseudoscalar glueball mass versus a^2 for both open (open symbols) and periodic (filled symbols) boundary conditions at Wilson flow time $\sqrt{8t} = 0.14$ fm. Also shown is the fit to the data.

plot the configuration average of the IPR versus Wilson flow time (t/a^2) in Fig. 11 for the ensembles P_1, P_2, and P_3. We note that $\langle \mathrm{IPR} \rangle$ monotonously decreases with decreasing flow time (t/a^2), indicating a reduced localization of $q(x)$. Also, *throughout* the range of t/a^2, $\langle \mathrm{IPR} \rangle$ appears to decrease with decreasing lattice spacing.

Since the Wilson flow provides a scale (independent of the lattice spacing) to probe the observables, it is more interesting to study the variation of $\langle \mathrm{IPR} \rangle$ with respect to $\sqrt{8t}$ for ensembles at different lattice spacings. In Fig. 12 we plot $\langle \mathrm{IPR} \rangle$ versus t/r_0^2 for ensembles P_1, P_2, and P_3. Remarkably, we find that—unlike the behavior shown in Fig. 11—the average IPRs for different ensembles are now very close to one another, and the average IPRs for the ensembles corresponding to the two smallest lattice spacings agree with each other within our statistical accuracy. The data for ensembles corresponding to the largest lattice spacing ($\beta = 6.21$) exhibits some mild scaling violation, as already noted in the case of the TCDC in Fig. 2. We note that, interestingly, the IPR is small for a small Wilson flow time and monotonously increases as the Wilson flow time increases. This indicates that when probed at short distances $q(x)$ is very much delocalized. On the other hand, when probed at long distances $q(x)$ appears more localized.

Among the available algebraic definitions for $q(x)$, one is based on the clover expression for the field strength $F_{\mu\nu}$, which is the simplest. Another is the more sophisticated ten-link definition developed for SU(2) by DeGrand, Hasenfratz, and Kovacs [43], which was modified for SU(3) by Hasenfratz and Neiter [44]. Also, there have been studies that employed tree-level improvement over the clover definition of $q(x)$ (as well as the action for the cooling process) in the case of SU(2) gauge theory [45]. In Fig. 13, we plot $\langle \mathrm{IPR} \rangle$ versus HYP sweeps using two definitions of the topological charge density (clover and ten link) for ensembles P_1, P_2, and P_3. It is expected that different lattice discretizations of the topological charge density yield the same physical observable as one approaches the continuum limit. We note that the $\langle \mathrm{IPR} \rangle$ for the two definitions of the topological charge density move closer to each other with decreasing lattice spacing, as expected.

We also note that $\langle \mathrm{IPR} \rangle$ decreases with decreasing lattice spacing at a given flow time. The behavior we have observed appears compatible with that exhibited by the data of the MILC Collaboration [32] at their three smallest lattice spacings. Note that the largest lattice spacing explored in our work is smaller than the smallest lattice spacing studied in Ref. [32] which, however, employed an improved lattice action.

In order to gain a better understanding of the behavior of both the charge density correlator $C(r)$ and the IPR, in Fig. 14 we plot the behavior of the topological charge density distribution $q(x)$ under the Wilson flow, as a function

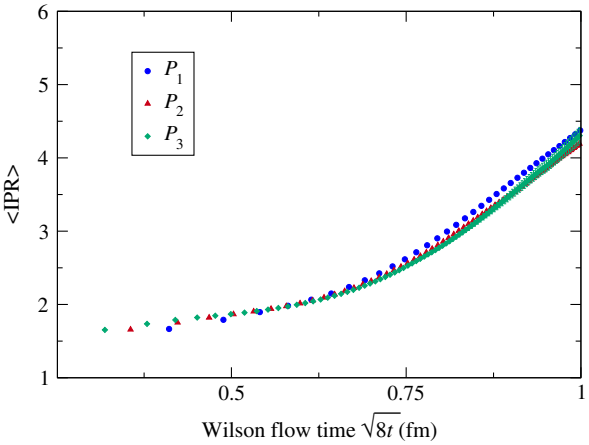

FIG. 12 (color online). $\langle \mathrm{IPR} \rangle$ versus $\sqrt{8t}$ for ensembles P_1, P_2, and P_3.

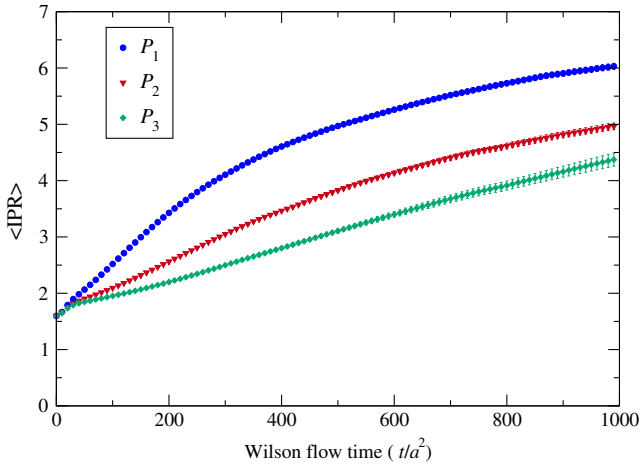

FIG. 11 (color online). Plot of the configuration average of the IPR ($\langle \mathrm{IPR} \rangle$) versus Wilson flow time (t/a^2) for the ensembles P_1, P_2, and P_3.

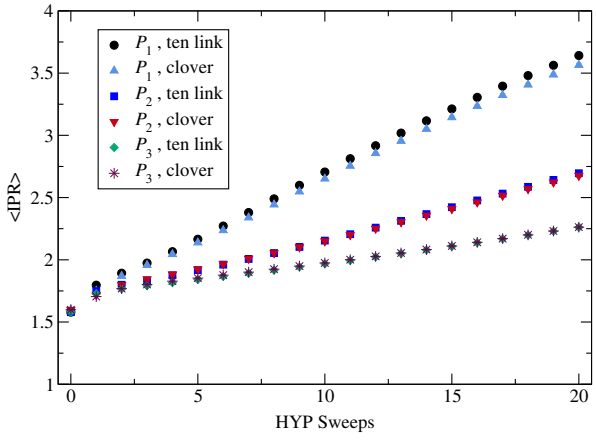

FIG. 13 (color online). Plot of $\langle \mathrm{IPR} \rangle$ versus HYP sweeps using two definitions of the topological charge density (clover and ten link) for ensembles P_1, P_2, and P_3.

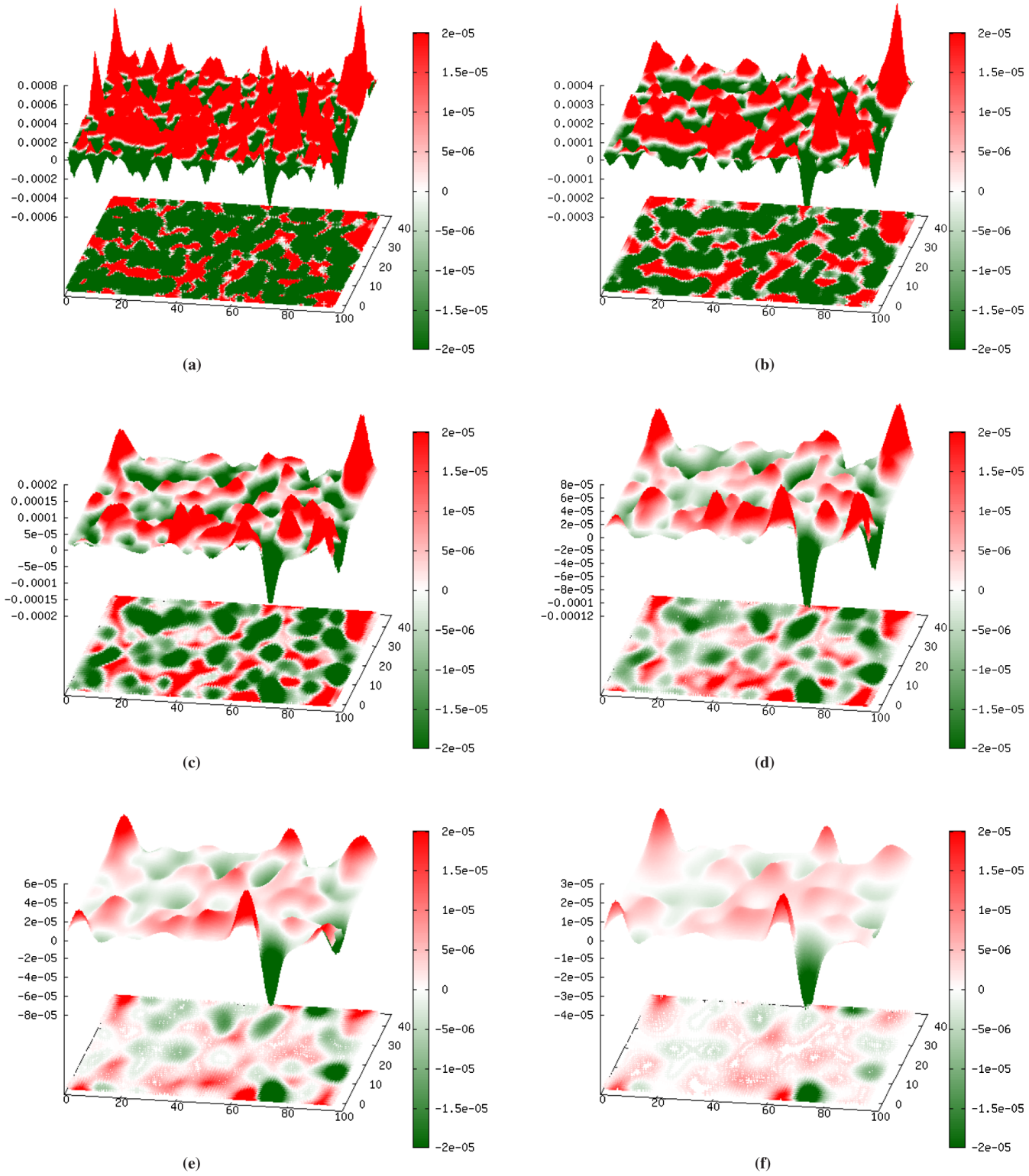

FIG. 14 (color online). The behavior of the topological charge density distribution $q(x)$ under the Wilson flow, as a function of x_0 and x_1 at $x_2 = x_3 = 24$ for a typical configuration belonging to the ensemble O_3. The plots (a)–(f) correspond to the flow times $\sqrt{8t} = 0.14$, 0.19, 0.25, 0.3, 0.38, and 0.47 fm, respectively.

of x_0 and x_1 at $x_2 = x_3 = 24$ for a typical configuration belonging to the ensemble O_3. Figures 14(a)–14(f) correspond to the flow times $\sqrt{8t} = 0.14$, 0.19, 0.25, 0.3, 0.38, and 0.47 fm, respectively. In the continuum, it is expected that the TCDC possesses a positive core and a negative peak that are adjacent to each other and close to the origin. This continuum behavior can be probed through the small values of the Wilson flow time. At relatively small values of the Wilson flow time, it is seen that $q(x)$ possesses regions of both positive and negative charge densities of relatively large magnitude that lie next to each other. This provides a qualitative explanation [46] of the positive core and the adjoining negative peak observed in $C(r)$. As the Wilson flow time decreases, the proximity of the regions of positive and negative charge densities of large magnitude increases, and the charge density appears to be more delocalized. This results in increased participation for $q(x)$, which in turn explains the decrease of the IPR with decreasing Wilson flow time, as discussed previously.

In the past, there have been studies (see, for example, Refs. [3,6,32]) of the fractal dimension of the topological charge density, which have used the Ginsparg-Wilson definition of the topological charge density and improved actions, but at considerably large lattice spacings compared to present standards. Our study of the IPR, on the other hand, has utilized the Wilson action at much smaller lattice spacings and the field strength definition of the topological charge density together with the Wilson flow to smooth the gauge configurations. It will be very interesting to extend the previous studies of the fractal dimension to much smaller lattice spacings together with the use of the Wilson flow to study the fractal dimension as a function of the flow time, in order to avoid any possible contamination of lattice artifacts so that one can reach definite conclusions. Our current study nevertheless seems to support the notion that the structure of the vacuum of Yang-Mills theory depends on the scale at which it is probed [31].

IV. CONCLUSIONS

In SU(3) lattice Yang-Mills theory, we have investigated the TCDC and IPR of the topological charge density $q(x)$ for a range of relatively small lattice spacings with the view of studying the continuum properties. As expected, we have not found any noticeable difference between the periodic and recently proposed open boundary conditions. However, the open boundary condition has enabled us to compute observables at a smaller lattice spacing because of the absence of the *trapping problem*. The recently proposed Wilson flow (in contrast to the smearing techniques proposed previously) provides a common energy scale to probe the system at a variety of lattice spacings. In contrast to a fixed HYP smearing level, by choosing a particular Wilson flow time t for all of the lattice spacings investigated, we find that—except for the data corresponding to the largest lattice spacing—the TCDC data show universal behavior within our statistical uncertainties. The continuum properties of the TCDC are inferred by studying the small-flow-time behavior. The pseudoscalar glueball mass obtained from the tail region of the TCDC does not exhibit any noticeable scaling violation and the extracted value in the continuum, 2563 (34) MeV, agrees well with the value extracted previously in the literature with anisotropic lattices. We found that the configuration average of the inverse participation ratio for the topological charge density, calculated at a given level of smearing (for the Wilson flow it is t/a^2) decreases with the lattice spacing. However, when plotted versus the common scale $\sqrt{8t}$, it seems to be independent of lattice spacing. A detailed study of $q(x)$ under the Wilson flow time revealed that as the Wilson flow time decreases, the proximity of the regions of positive and negative charge densities of large magnitude increases, and the charge density appears to be more delocalized, resulting in the observed decrease of the IPR with decreasing Wilson flow time.

ACKNOWLEDGMENTS

To carry out all the numerical calculations reported in this work, Cray XT5 and Cray XE6 systems supported by the 11th-12th Five Year Plan Projects of the Theory Division, SINP under the Department of Atomic Energy, Govt. of India, were used. We thank Richard Chang for the prompt maintenance of the systems and helping with data management. For some useful discussions, we also thank Pushan Majumdar and Santanu Mondal. We are indebted to Philippe de Forcrand for helpful comments on the earlier version of this manuscript. This work was in part based on the publicly available lattice gauge theory code OPENQCD [47] and that of the MILC Collaboration [48].

[1] E. Seiler and I. O. Stamatescu, Some remarks on the Witten-Veneziano formula for the eta-prime mass, Report No. MPI-PAE/PTh10/87 (unpublished).

[2] E. Seiler, Some more remarks on the Witten-Veneziano formula for the eta-prime mass, Phys. Lett. B **525**, 355 (2002).

[3] I. Horvath, S. J. Dong, T. Draper, F. X. Lee, K. F. Liu, N. Mathur, H. B. Thacker, and J. B. Zhang, Low dimensional long range topological charge structure in the QCD vacuum, Phys. Rev. D **68**, 114505 (2003).
[4] A. Hasenfratz, Spatial correlation of the topological charge in pure SU(3) gauge theory and in QCD, Phys. Lett. B **476**, 188 (2000).
[5] I. Horvath, A. Alexandru, J. B. Zhang, Y. Chen, S. J. Dong, T. Draper, K. F. Liu, N. Mathur, S. Tamhankar, and H. B. Thacker, The negativity of the overlap-based topological charge density correlator in pure-glue QCD and the non-integrable nature of its contact part, Phys. Lett. B **617**, 49 (2005).
[6] E.-M. Ilgenfritz, K. Koller, Y. Koma, G. Schierholz, T. Streuer, and V. Weinberg, Exploring the structure of the quenched QCD vacuum with overlap fermions, Phys. Rev. D **76**, 034506 (2007).
[7] E.-M. Ilgenfritz, D. Leinweber, P. Moran, K. Koller, G. Schierholz, and V. Weinberg, Vacuum structure revealed by over-improved stout-link smearing compared with the overlap analysis for quenched QCD, Phys. Rev. D **77**, 074502 (2008); Phys. Rev. D **77**, 099902(E) (2008).
[8] P. J. Moran and D. B. Leinweber, Impact of dynamical fermions on QCD vacuum structure, Phys. Rev. D **78**, 054506 (2008).
[9] A. Bazavov *et al.* (MILC Collaboration), Topological susceptibility with the asqtad action, Phys. Rev. D **81**, 114501 (2010).
[10] F. Bruckmann, F. Gruber, N. Cundy, A. Schafer, and T. Lippert, Topology of dynamical lattice configurations including results from dynamical overlap fermions, Phys. Lett. B **707**, 278 (2012).
[11] A. Chowdhury, A. K. De, A. Harindranath, J. Maiti, and S. Mondal, Topological charge density correlator in lattice QCD with two flavors of unimproved Wilson fermions, J. High Energy Phys. 11 (2012) 029.
[12] M. Bruno, S. Schaefer, and R. Sommer, Topological susceptibility and the sampling of field space in $N_f = 2$ lattice QCD simulations, J. High Energy Phys. 08 (2014) 150.
[13] H. Fukaya *et al.* (JLQCD Collaboration), Topology density correlator on dynamical domain-wall ensembles with nearly frozen topological charge, in *Proceedings of the 32nd International Symposium on Lattice Field Theory (Lattice 2014)*, (New York, NY, June 23–28, 2014) (to be published), arXiv:1411.1473.
[14] E. Witten, Current algebra theorems for the U(1) Goldstone boson, Nucl. Phys. **B156**, 269 (1979).
[15] G. Veneziano, U(1) without instantons, Nucl. Phys. **B159**, 213 (1979).
[16] S. Dürr, Z. Fodor, C. Hoelbling, and T. Kurth, Precision study of the SU(3) topological susceptibility in the continuum, J. High Energy Phys. 04 (2007) 055.
[17] L. Del Debbio, L. Giusti, and C. Pica, Topological susceptibility in the SU(3) gauge theory, Phys. Rev. Lett. **94**, 032003 (2005).
[18] M. Luscher, Topological effects in QCD and the problem of short distance singularities, Phys. Lett. B **593**, 296 (2004).
[19] L. Giusti and M. Luscher, Chiral symmetry breaking and the Banks-Casher relation in lattice QCD with Wilson quarks, J. High Energy Phys. 03 (2009) 013.
[20] M. Lüscher and F. Palombi, Universality of the topological susceptibility in the SU(3) gauge theory, J. High Energy Phys. 09 (2010) 110.
[21] M. Lüscher, Topology, the Wilson flow and the HMC algorithm, *Proc. Sci.*, LATTICE (2010) 015 [arXiv: 1009.5877].
[22] M. Lüscher and S. Schaefer, Lattice QCD without topology barriers, J. High Energy Phys. 07 (2011) 036.
[23] M. Lüscher and S. Schaefer, Lattice QCD with open boundary conditions and twisted-mass reweighting, Comput. Phys. Commun. **184**, 519 (2013).
[24] M. Grady, Connecting phase transitions between the 3-d O(4) Heisenberg model and 4-d SU(2) lattice gauge theory, arXiv:1104.3331.
[25] A. Hasenfratz and F. Knechtli, Flavor symmetry and the static potential with hypercubic blocking, Phys. Rev. D **64**, 034504 (2001).
[26] M. Lüscher, Trivializing maps, the Wilson flow and the HMC algorithm, Commun. Math. Phys. **293**, 899 (2010).
[27] M. Lüscher, Properties and uses of the Wilson flow in lattice QCD, J. High Energy Phys. 08 (2010) 071.
[28] M. Lüscher and P. Weisz, Perturbative analysis of the gradient flow in non-abelian gauge theories, J. High Energy Phys. 02 (2011) 051.
[29] A. Chowdhury, A. Harindranath, J. Maiti, and P. Majumdar, Topological susceptibility in lattice Yang-Mills theory with open boundary condition, J. High Energy Phys. 02 (2014) 045.
[30] A. Chowdhury, A. Harindranath, and J. Maiti, Open boundary condition, Wilson Flow and the scalar Glueball mass, J. High Energy Phys. 06 (2014) 067.
[31] For a review, see P. de Forcrand, Localization properties of fermions and bosons, AIP Conf. Proc. **892**, 29 (2007).
[32] C. Aubin, C. Bernard, S. Gottlieb, E.B. Gregory, Urs M. Heller, J.E. Hetrick, J. Osborn, R. Sugar, P. de Forcrand, and O. Jahn (MILC Collaboration), The scaling dimension of low lying Dirac eigenmodes and of the topological charge density, Nucl. Phys. B, Proc. Suppl. **140**, 626 (2005).
[33] M. Guagnelli, R. Sommer, and H. Wittig (ALPHA Collaboration), Precision computation of a low-energy reference scale in quenched lattice QCD, Nucl. Phys. **B535**, 389 (1998).
[34] S. Necco and R. Sommer, The $N_f = 0$ heavy quark potential from short to intermediate distances, Nucl. Phys. **B622**, 328 (2002).
[35] C. Bonati and M. D'Elia, Comparison of the gradient flow with cooling in SU(3) pure gauge theory, Phys. Rev. D **89**, 105005 (2014).
[36] M. Creutz, Anomalies, gauge field topology, and the lattice, Ann. Phys. (N.Y.) **326**, 911 (2011).
[37] Y. Chen *et al.*, Glueball spectrum and matrix elements on anisotropic lattices, Phys. Rev. D **73**, 014516 (2006).
[38] E. V. Shuryak and J. J. M. Verbaarschot, Screening of the topological charge in a correlated instanton vacuum, Phys. Rev. D **52**, 295 (1995).

[39] C. Rosenzweig, J. Schechter, and C. G. Trahern, Is the effective lagrangian for QCD a sigma model?, Phys. Rev. D **21**, 3388 (1980).
[40] P. Di Vecchia and G. Veneziano, Chiral dynamics in the large N limit, Nucl. Phys. **B171**, 253 (1980).
[41] R. J. Bell and R. Dean, Atomic vibrations in vitreous silica, Discuss. Faraday Soc. **50**, 55 (1970).
[42] F. Wegner, Inverse participation ratio in $2+\epsilon$ dimensions, Z. Phys. B **36**, 209 (1980).
[43] T. A. DeGrand, A. Hasenfratz, and T. G. Kovacs, Topological structure in the SU(2) vacuum, Nucl. Phys. **B505**, 417 (1997).
[44] A. Hasenfratz and C. Nieter, Instanton content of the SU(3) vacuum, Phys. Lett. B **439**, 366 (1998).
[45] P. de Forcrand, M. Garcia Perez, and I. O. Stamatescu, Topology of the SU(2) vacuum: A Lattice study using improved cooling, Nucl. Phys. **B499**, 409 (1997).
[46] S. Ahmad, J. T. Lenaghan, and H. B. Thacker, Coherent topological charge structure in $CP^{(N-1)}$ models and QCD, Phys. Rev. D **72**, 114511 (2005).
[47] http://luscher.web.cern.ch/luscher/openQCD/.
[48] http://physics.indiana.edu/~sg/milc.html.